Taylor & Francis
Taylor & Francis Group

Strategies for Imaging Diffusing Media

Randall L. Barbour

Department of Pathology, SUNY Downstate Medical Center, Brooklyn,
NY, USA and NIRx Medical Technologies LLC., Glen Head, NY, USA

Harry L. Graber and Yong Xu

Department of Pathology, SUNY Downstate Medical Center, Brooklyn,
NY, USA

Yaling Pei and Raphael Aronson

NIRx Medical Technologies LLC., Glen Head, NY, USA

Abstract: We present a new approach to improving images in diffusion tomography, involving construction of a linear filter function that converts images of absorption and scattering coefficients back into the initial configuration being imaged. In a practical situation, the initial configuration is not known, so that the filter function is constructed by simulation for a neighboring situation. The algorithm is quite robust, so that the neighboring situation need not be all that close to that of interest. We show how to construct such a filter and give illustrations of how well it solves the problem. In one configuration shown, this procedure gives a better image than 50 Born iterations. This suggests that the inherent nonlinearity of the problem in diffusion tomography may not be the largest source of error, but that linear errors may be more important. A crucial advantage of the filter procedure is that the filter (or preferably, library of filters) can be computed before the experiment of interest. It is only inversion of the pattern of detector readings and application of the filter that take place afterward, and both are very fast, leading to enhanced images in what is essentially real time.

Keywords: Medical and biological imaging, image reconstruct techniques, deconvolution, tomographic image processing

Address correspondence to Randall L. Barbour, Department of Pathology, SUNY Downstate Medical Center, Box 25, 450 Clarkson Avenue, Brooklyn, NY 11203, USA. E-mail: randall.barbour@downstate.edu

1.   INTRODUCTION

One significant application of transport theory over the past 15 years or so has been to near-infrared medical imaging (Aronson et al. 1991; Müller et al. 1993; Minet, Müller, and Beuthan 1998; Chance et al. 2003). This rapidly growing field has gone by the name of diffusion tomography, and in the opinion of many, it is destined to become a big technology.

Described as a physical and mathematical problem, the idea is that there are a number of sources and detectors placed on the surface of the object, a breast or head or whatever part of the body is to be imaged. One sends in laser beams at one or more wavelengths and measures the radiation scattered into the detectors from the object. One then solves an inverse problem for the absorption and possibly the scattering coefficient as a function of position in the interior, at each wavelength. The inversion is based on a linear technique, while the coefficients and the detector readings are related nonlinearly. The resulting image, as shown in some of the figures below for sample problems, is often very poor. The results can be used to recalculate the parameters entering into the inversion in order to invert again to get an updated image. This iteration often has to be done many times to get a good image (Jiang et al. 1998; Schweiger and Arridge 1998).

We now describe a new and very different approach to improving the initial image, using a linear filter approach.

2.   METHODS

A typical experiment employs a number of sources and detectors. The sources are activated in sequence by switches, and all of them are sampled several times a second. All the detectors read the results from each source. We get a time series of results by going through many cycles. Of course there is noise from several causes. Now suppose that the cross sections in each voxel were to vary sinusoidally in time, with a different frequency in each (two different frequencies if we want scattering as well as absorption). If there were no errors in the measurements and if we had an exact reconstruction and looked at the frequency spectrum, we would find the cross sections for each voxel oscillating at the respective input frequencies. (Technical point: We choose the frequencies to be incommensurable so that one of them does not also show up in the results due to sums or differences of input frequencies.) This does not happen so neatly in practice, of course. At each frequency the reconstruction gives a spread of perturbed cross sections of various strengths in voxels other than the input voxel for that frequency. Typically these are nearby voxels. This spread can be represented by a matrix, giving the strengths of the reconstructed perturbed cross section found for each voxel, for each original voxel. Presumably inverting this matrix will furnish a filter that we can expect to clean up the reconstruction to give more exact results. Now this is a calculated filter matrix.

If the calculated situation is close enough to the experimental situation, this filter presumably improves the reconstruction from the experiment as well.

For reasons not yet fully worked out, this scheme was not really successful, while working with the time series directly rather than with the frequency transforms was much better. For that reason, the rest of this paper will use the language of time series. For simplicity, we consider a case in which the scattering cross section is constant and known, so that only the absorption cross section needs to be examined.

Thus consider N voxels with incommensurate sinusoidally varying cross sections. The forward calculation is done at T times that differ by a small fraction of the smallest oscillation period, but over many cycles of the longest period, and each forward calculation is inverted to give a calculated value of the cross section for each voxel. The input can be described by a set of quantities y_{nt}, where n is the voxel number and t the time index. This information can be collected in an $N \times T$ matrix $\mathbf{Y}$. Similarly, the reconstructed cross sections can be described by quantities x_{nt}, which can be considered as elements of an $N \times T$ matrix $\mathbf{X}$. We want to determine an $N \times N$ filter matrix $\mathbf{F}$ that transforms $\mathbf{X}$ back into $\mathbf{Y}$. That is, we would like to solve the equation $\mathbf{Y} = \mathbf{FX}$. We will then take this $\mathbf{F}$ and apply it to reconstructed experimental images, in the hope of improving them.

Now $\mathbf{X}$ and $\mathbf{Y}$ are in general not square matrices, since $T \gg N$ in the situations of interest, and so they cannot in general be inverted. The calculations whose results are shown here used 717 voxels and 16,384 (2^{14}) time steps. In fact, in general the equation $\mathbf{Y} = \mathbf{FX}$ cannot hold. This situation is common in statistical problems. The matrix equation represents T linear equations in N unknowns, and unless the coefficients are linearly dependent in some way, there is no exact solution. We therefore approximate the matrix equation as well as possible in a least-squares sense. That is, we choose the elements f_{nm}, of $\mathbf{F}$ to minimize the quantity

$$I = \sum_{t=1}^{T} \sum_{n=1}^{N} \left(y_{nt} - \sum_{m=1}^{N} f_{nm} x_{mt} \right)^2,$$

which gives the sum of the squares of the errors in the individual terms in approximating $\mathbf{Y}$ by $\mathbf{FX}$. Putting the derivative of I with respect to each element of $\mathbf{F}$ equal to zero gives

$$\partial I / \partial f_{nm} = -2 \sum_{t=1}^{T} \left(y_{nt} - \sum_{k=1}^{N} f_{nk} x_{kt} \right) x_{mt} = 0.$$

This is just the matrix equation

$$\mathbf{Y}\mathbf{X}^{\mathrm{T}} = \mathbf{F}\mathbf{X}\mathbf{X}^{\mathrm{T}},$$

where $\mathbf{X}^T$ is the transpose of $\mathbf{X}$. Since $\mathbf{XX}^T$ is a square matrix, it can be inverted in general to give

$$\mathbf{F} = (\mathbf{YX}^T)(\mathbf{XX}^T)^{-1}.$$

There is nothing original about this. It is just a linear regression procedure. Note that if one wants to invert the procedure, trying to approximate $\mathbf{X} = \mathbf{GY}$, one finds that

$$\mathbf{G} = (\mathbf{XY}^T)(\mathbf{YY}^T)^{-1},$$

and in general, $\mathbf{F}$ and $\mathbf{G}$ are not inverses of each other.

To make this a little more concrete, Figure 1 shows a typical $\mathbf{G}$ filter for a two-dimensional problem that gives the transformation of input information to output information. It looks like a fuzzy identity matrix, which one might expect. It's somewhat more complicated because of course in two dimensions integers can't be well ordered, so for the most part next to a voxel with any given number there are other voxels with numbers far removed. The graph would not look really closely diagonal even if there were communication only with nearest neighbors.
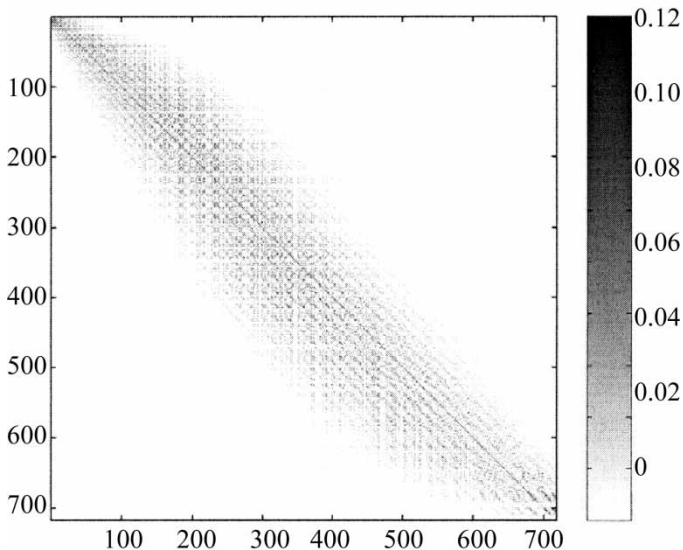
Figure 1.   Typical **G**-matrix.

3. RESULTS AND DISCUSSION

The remainder of the figures in this paper involve one or the other of two different 2-D geometries. Both are for a circular region 8 cm in diameter with uniform cross sections except for certain identical circular inclusions with different absorption properties, located symmetrically about the center, each 0.6 cm in diameter with center 1.5 cm from the center of the circle. The background scattering and absorption coefficients are $\mu_s = 10\,\text{cm}^{-1}$ and, $\mu_a = 0.05\,\text{cm}^{-1}$, respectively. In the inclusions, the scattering coefficient is the same, but the absorption coefficient is either $0.06\,\text{cm}^{-1}$ or $0.40\,\text{cm}^{-1}$.

In the first situation, shown diagrammatically in Figure 2, there are four inclusions. Sixteen sources and 16 detectors are located uniformly around the circumference, with sources and detectors interspersed. Whether they are interspersed or located in the same positions is actually not important, provided that there are enough of them. We have also done calculations
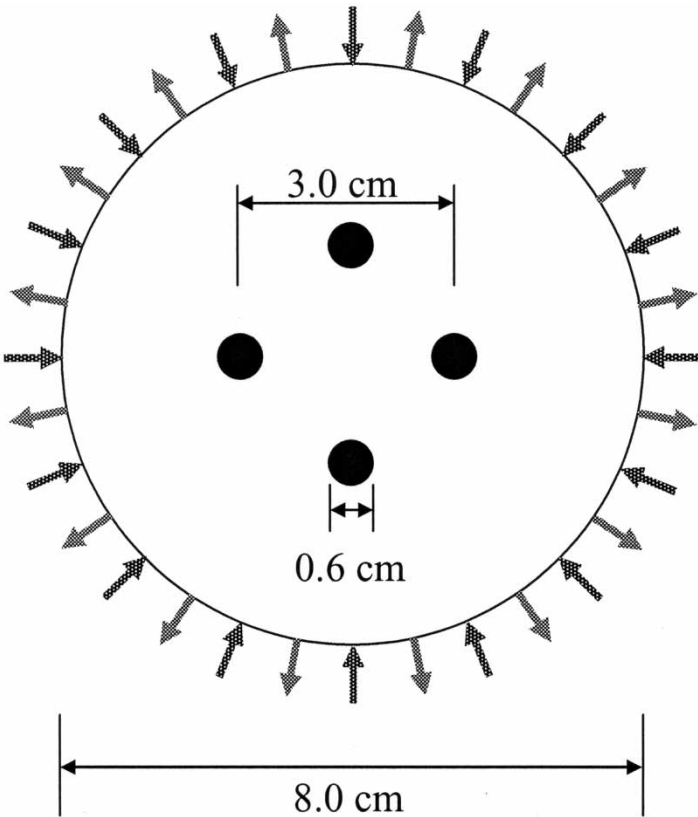
Figure 2.   Schematic four-inclusion geometry, full view.

(a): $\mu_a = 0.06$ cm^{-1},
16 sources (S),
16 detectors (D)

(b): $\mu_a = 0.4$ cm^{-1},
16 S, 16 D

(c): $\mu_a = 0.4$ cm^{-1},
32 S, 32 D

(d): $\mu_a = 0.06$ cm^{-1},
16 S, 16 D

(e): $\mu_a = 0.4$ cm^{-1},
16 S, 16 D

(f): $\mu_a = 0.4$ cm^{-1},
32 S, 32 D
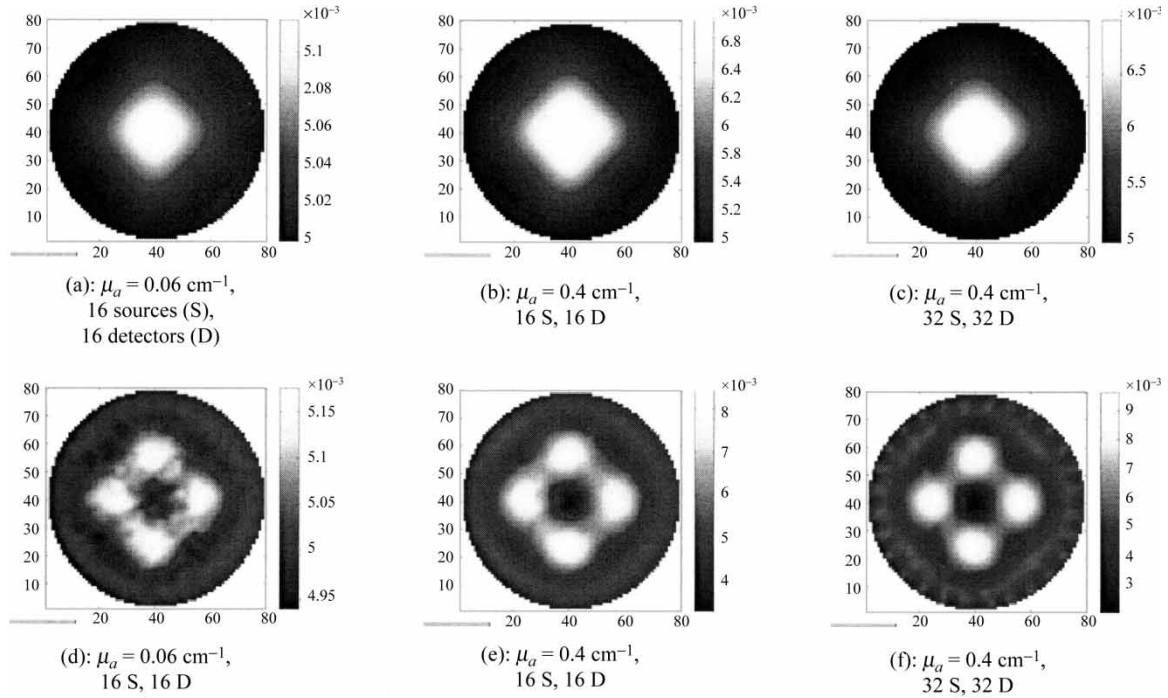
Figure 3. Demonstration of image-enhancing (spatial deconvolution) effect of the filter matrix **F**. Reconstructed images of four-inclusion (Figure 2) target media are shown, for inclusion μ_a values of 0.06 cm^{-1} and 0.4 cm^{-1} (background $\mu_a = 0.05$ cm^{-1}). The images produced by applying the filter matrix to the results in the top row are shown in the second row, for μ_a values of 0.06 cm^{-1} and 0.4 cm^{-1}.

with 8 sources and 8 detectors and with 32 sources and 32 detectors. The results are quite similar.

Figure 3(a) shows results of the inversion for 16 sources and 16 detectors (16 × 16) for $\mu_a = 0.06\,\mathrm{cm}^{-1}$, Figure 3(b) for l6 × 16 and $\mu_a = 0.40\,\mathrm{cm}^{-1}$, and Figure 3(c) for 32 × 32 and $\mu_a = 0.4\,\mathrm{cm}^{-1}$. The fourfold symmetry is apparent, but little else of the structure. Figures 3(d)–3(f) have the same source-detector numbers and absorption coefficients as Figures 3(a)–3(c), respectively. Each results from its respective parent by applying a filter matrix **F** for a circular region consisting of background only. The inclusions show clearly in the filtered images.

A second geometry we examined is the limited-view geometry shown in Figure 4. This is interesting because usually only a limited view is available in clinical situations. There are nine sources and 24 detectors, located uniformly on only half of the circumference, and two inclusions.
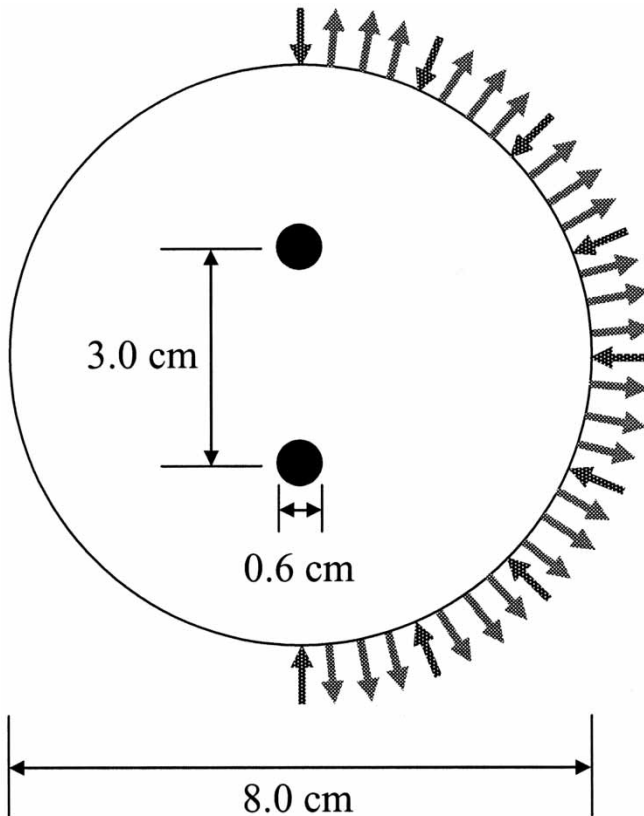
Figure 4.   Schematic two-inclusion geometry, limited view.

(a): $\mu_a = 0.06$ cm^{-1},
without filter

(b): $\mu_a = 0.4$ cm^{-1},
without filter

(c): $\mu_a = 0.06$ cm^{-1},
with filter

(d): $\mu_a = 0.4$ cm^{-1},
with filter
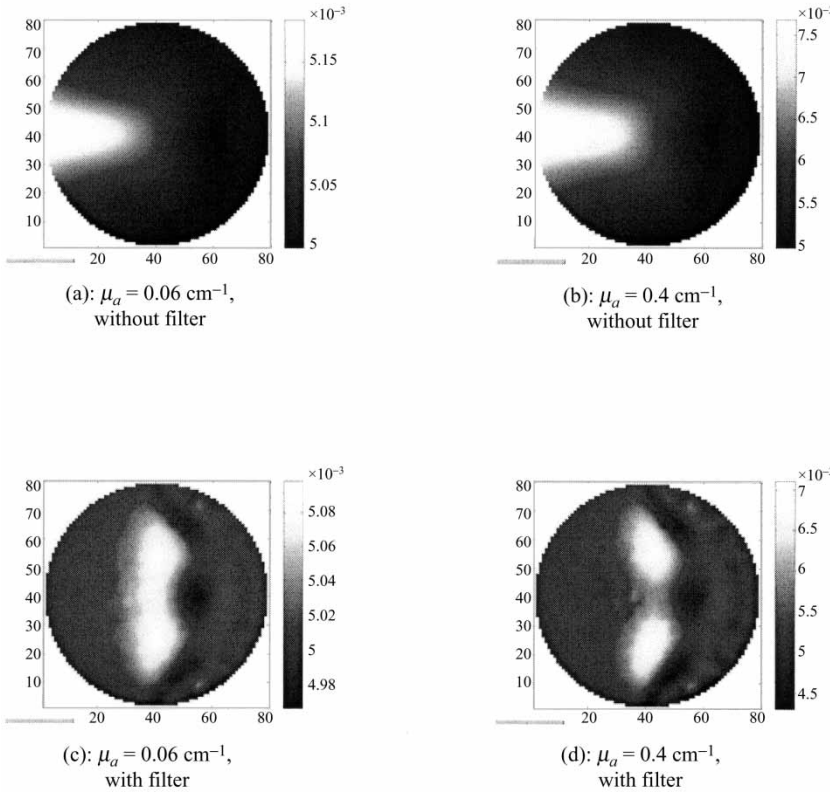
Figure 5. Demonstration of image-enhancing (spatial deconvolution) effect of the filter matrix **F**. Reconstructed images of two-inclusion, limited-view (Figure 4) target media are shown, for inclusion μ_a values of 0.06 cm^{-1} and 0.40 cm^{-1} (background $\mu_a = 0.05$ cm^{-1}). The images produced by applying the filter matrix to the results in the top row are shown in the second row, for μ_a values of 0.06 cm^{-1} and 0.40 cm^{-1}.

Figures 5(a) and 5(b) show unfiltered images, 5(c) and 5(d) the corresponding filtered images. In Figures 5(a) and 5(c), $\mu_a = 0.06$ cm^{-1} in the inclusions; in Figures 5(b) and 5(d), $\mu_a = 0.40$ cm^{-1}. Without the filter one sees just the symmetry with respect to a horizontal diameter. The other features are due to the placement of the sources and detectors on the right of the configuration. The computed absorptions with no filter are much higher on the side away from the sources and detectors. The inclusions aren't seen at all. Evidently the image depends strongly on the placement of the sources and detectors, and very little on the structure of the medium. This is not true for the filtered images, which show the inclusions clearly.

To bring out even more strongly the advantages of using the filter, we compared the effect of applying the filter to a first-order image with the results
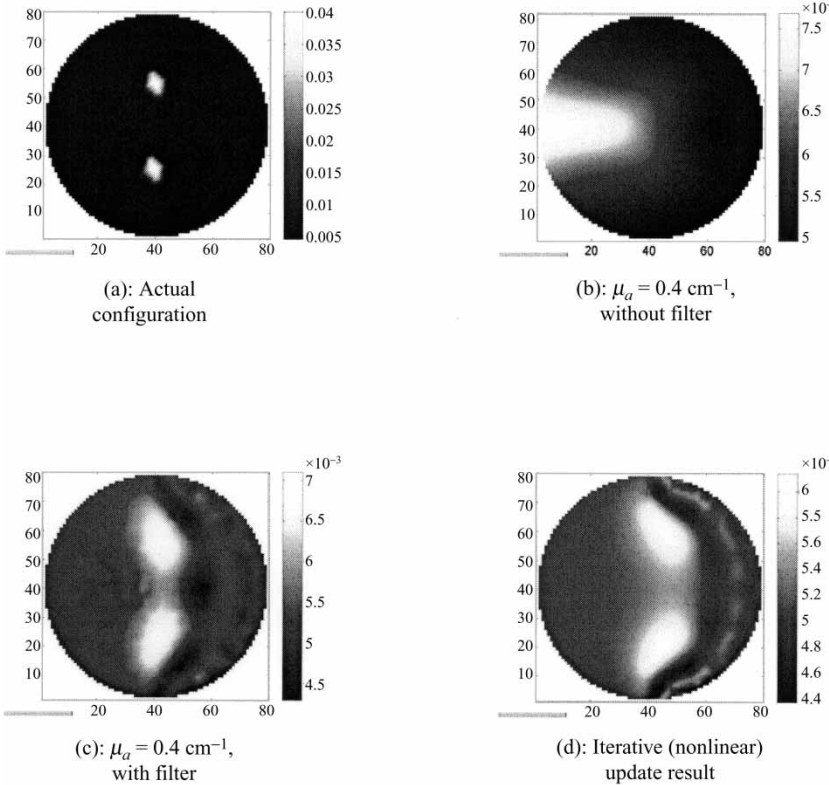
Figure 6. Comparison of filter-enhanced reconstructed image of two-inclusion, limited-view (Figure 4) target medium, for inclusion μ_a values of $0.04\,\text{cm}^{-1}$ (backgroud $\mu_a = 0.05\,\text{cm}^{-1}$), and reconstructed image of the same target medium after 50 cycles of a Born iterative reconstruction algorithm. Unfiltered (i.e., first iteration) reconstructed image and original target medium also are shown.

of using a Born iterative algorithm for the geometry of Figure 4 for $\mu_a = 0.40\,\text{cm}^{-1}$. Figure 6(a) is the initial configuration, the one to be imaged. It looks a little unlike the idealized Figure 4 because it is generated by the initial numerical approximation necessitated by the discrete algorithm involved in our finite element scheme. Figure 6(b) shows the first-order image and is identical with Figure 5(b). Figure 6(c) is the filtered image and is identical with Figure 5(d). Figure 6(d) is the result of iterating 50 times without a filter.

The two results look qualitatively similar, but the filtered one is altogether superior. It is much more symmetric about the vertical diameter; the inclusions are accurately located, which they are not in the other; and the resolution is

better. Calculation of the 50 iterations takes about three hours on the desktop computer used, and it all has to be done after the experiment (here a simulation). Calculation of the filter is faster, though of the same order of magnitude, but postprocessing requires only about 100 ms on the same computer. Further work has shown that the filter method is remarkably robust. That is, the medium for which the filter is computed does not have to be awfully similar to the actual medium to get good results.

Finally, one really significant and surprising realization arises from the superiority of the filter method in the cases examined. It was always thought that the major inaccuracies in diffusion tomography come from the fact that the detector readings are nonlinear in the absorption and scattering coefficients (Ostermeyer and Jacques 1997). The iterations are intended to take account of this inherent nonlinearity. The success of the filter technique, which is linear, suggests that the nonlinearities may not be as large a source of error as errors inherent in the calculation itself, such as in the discretization. It is certainly possible that the same situation holds for other physical problems and that a filter technique of the sort described here will have much broader application. If the filter method continues to be successful in important cases, one can envision building a library of filter matrices for a large number of situations, so that in a clinical situation one can hope to find one that fits the experimental situation rather closely.

ACKNOWLEDGMENTS

REFERENCES

Aronson, R., Barbour, R. L., Lubowsky, J., Graber, H. L. (1991). Application of transport theory to infra-red medical imaging. *Operator Theory: Advances and Applications*, Vol. 51. 11th International Conference on Transport Theory, Blacksburg, VA, May 22–26, 1989, Basel, Switzerland: Birkhäuser Verlag Press.

Chance, B., Alfano, R. R., Tromberg, B. J., Tamura, M., Sevick-Muraca, E. M. Eds. (2003). *Optical Tomography and Spectroscopy of Tissue V*. (Proceedings of the BiOS 2003 Conference, San Jose, Calif, Jan 25–31, 2003), Bellingham, Wash: Society of Photo-Optical Instrumentation Engineers.

Jiang, H., Paulsen, K. D., Osterberg, U. L., Patterson, M. S. (1998). Improved continuous light imaging in single- and multi-target tissue-like phantoms. *Physics in Medicine and Biology* 43:675–693.

Minet, O., Müller, G., Beuthan, J. Eds. (1998). *Selected Papers on Optical Tomography Fundamentals and Applications in Medicine*. SPIE Milestone Series,

Vol. MS 147. Bellingham, Wash: Society of Photo-Optical Instrumentation Engineers.

Müller, G., Chance, B., Alfano, R., Arridge, S., Beuthan, J., Gratton, E., Kaschke, M., Masters, B., Svanberg, S., van der Zee, P. Eds. (1993). *Medical Optical Tomography: Functional Imaging and Monitoring*. Vol. IS 11. Bellingham, Wash: SPIE Institutes.

Ostermeyer, M. R., Jacques, S. L. (1997). Perturbation theory for diffuse light transport in complex biological tissues. *J. Optical Society of America A* 14:255–261.

Schweiger, M., Arridge, S. R. (1998). Comparison of two- and three-dimensional reconstruction methods in optical tomography. *Applied Optics* 37:7419–7428. . and provide email..